J Mater Sci: Mater Med (2011) 22:1137–1146
DOI 10.1007/s10856-011-4303-x

A pictographic atlas for classifying damage modes on polyethylene bearings

Melinda Harman · Luca Cristofolini · Paolo Erani · Susanna Stea · Marco Viceconti

Received: 4 November 2010 / Accepted: 21 March 2011 / Published online: 2 April 2011

Abstract Evaluation of medical devices retrieved after in vivo service provides unique evidence related to the physiological environment in which the biomaterials performed. This study implements a training procedure for evaluating polyethylene bearings of joint prostheses obtained after pre-clinical tests or explanted after in vivo function. A total of 161 damage regions on 45 bearings were evaluated by four observers. An illustrated Damage Mode Atlas was developed as a reference guide, inclusive of both photographs and concise written descriptions of 16 specific damage modes that are typical for polyethylene bearings. Utilizing the Damage Mode Atlas to train new researchers improved the damage pattern analysis, including more accurate identification of damage modes and improved inter-rater reliability. This Damage Mode Atlas is a useful supplementary tool for conducting Stage II non-destructive analysis of explanted polyethylene bearings used for joint replacement, in accordance with international guidelines for evaluating explanted medical devices.

1 Introduction

Wear of the metal-polyethylene bearing couple in joint replacements continues to drive changes in bearing materials, designs and manufacturing processes [1–3]. Different articular wear mechanisms correspond to visibly different damage patterns on retrieved polyethylene bearings [4–14] and varied clinical outcomes [15–22]. During in vitro functional simulations of joint prostheses, damage patterns reflect the performance of the bearing couple under the applied kinematics and loading conditions [23–31]. Therefore, analysis of damage patterns on bearing couples used in joint prostheses has proven complementary to both post-marketing surveillance and pre-clinical assessments.

Damage patterns on worn polyethylene bearings can be characterized using visual recognition of specific damage modes [4, 13, 32, 33]. The distinguishing features of different damage modes typically are visible at low magnification using optical microscopy. However, uniform descriptions and reference illustrations of actual damage modes can be difficult to gather from the scientific literature and terminology for describing the distinguishing features is inconsistent, often varying with analysis methods [14, 29]. This lack of standardized reference materials for identifying specific damage modes on polyethylene bearings makes it difficult to train new observers and assure repeatable assessment of the damage patterns.

The purpose of this study was to implement a training procedure for identifying damage modes, as is necessary for completing damage pattern analysis on polyethylene bearings from joint prostheses. The first objective was to create an illustrated reference guide of damage modes (Damage Mode Atlas) that are typically visualized on polyethylene bearings. The second objective was to use the Damage Mode Atlas for training new researchers, determining the intra-observer accuracy and inter-observer reproducibility for damage mode identification. It was hypothesized that training with the Damage Mode Atlas would improve the accuracy and reproducibility for visually identifying damage modes on explanted polyethylene

M. Harman · L. Cristofolini (✉) · P. Erani · S. Stea · M. Viceconti
Medical Technology Lab, Rizzoli Orthopaedic Institute, Via di Barbiano 1/10, 40136 Bologna, Italy
e-mail: cristofolini@tecno.ior.it

L. Cristofolini
Engineering Faculty, University of Bologna, Bologna, Italy

bearings compared to training based on written descriptions alone.

2 Methods

Polyethylene bearings were explanted during revision arthroplasty at one institution (Rizzoli Orthopaedic Institute, Bologna, Italy) and cataloged in a Register of Orthopaedic Prosthetic Explants. The bearings were cleaned by submersion in an enzymatic detergent (Dialzima H) solution (0.5% v/v) for 12 h to remove organic debris, sterilized by submersion in formalin (4% v/v) for 24 h and then allowed to air dry. One researcher (MKH) experienced in evaluating damage on polyethylene bearings assessed the bearing surfaces using visual identification techniques [4–6, 23] and an optical microscope (SMZ-2T, Nikon Corp., Tokyo, Japan) allowing visualization under reflected and transmitted light conditions. The microscope was fitted with lenses providing magnification $\times 10$ to $\times 126$, an auxiliary flexible illuminator (model GKL 315, Gossen Photo and Light Measurement GmbH, Nürnberg, Germany), and a ring illuminator (model MA964/TF, Meiji Techno Co. Ltd., Saitama, Japan). A group of 45 bearings from knee prostheses were selected for inclusion in this study based on visual evidence of 16 specific damage modes. These modes are recognized as typically occurring on polyethylene bearings with low to moderate conformity (e.g. knee or shoulder prostheses) and are readily observed with optical microscopy [4–6, 13, 23, 33].

An illustrated Damage Mode Atlas (Figs. 1, 2, 3, Tables 1, 2) was created by integrating both photographs and written descriptions of the 16 specific damage modes. There were ten modes consistent with adhesive/abrasive or fatigue mechanisms that can occur with cyclic loading of polyethylene bearings [4–9, 11–15, 23–25, 32, 33, 35, 36], three modes characteristic of damage on the non-articular (backside) surface of modular bearings [5, 9, 34–36], and three modes characteristic of common artifacts originating during surgery or manufacturing. Representative regions characteristic of the 16 specific damage modes were identified visually and photographed using a high resolution digital imaging system (D80 camera and AF-S MicroNikkor lens, Nikon Corp., Tokyo, Japan) with controlled illumination and uniform magnification (Figs. 1, 2). The images were originally captured as black and white 24 bit JPEG format containing 3872 $\times$ 2592 pixels per image. Image resolution was controlled using a standard photogrammetric reference scale (ABFO No. 2) [37] and averaged 400 pixels/mm when acquired through the optical microscope and 80 pixels/mm when acquired as a macro photo.

The written descriptions of each damage mode included their appearance under reflected light illumination, recognized mechanisms that potentially contribute to the damage modes and five distinguishing features that can be readily observed at low magnifications. The visual appearance and typical damage mechanisms (Tables 1, 2) are consistent with distinct features elaborated in previous studies using low magnification identification of damage morphology [4–6, 8, 9, 11–15, 23–25, 32–36]. The features included relative size, variations in color, texture and reflectivity, and typical locations in which the damage mode appears on the bearing surfaces. Relative size was characterized as macro (i.e. visible to the unaided eye) or micro (i.e. best visualized using microscopy). Variations in color were characterized as absent (i.e. uniform color) or present (i.e. change in polyethylene color or opacity). Variations in texture were assessed relative to the original bearing surface and were characterized as smooth (i.e. visibly less textured) or rough (i.e. visibly more textured). Variations in reflectivity were determined by the behavior of the incidence light beam under the microscope and were characterized as low or high. Finally, locations in which the damage modes typically occur were characterized as articular (i.e. the surfaces that are intended to endure articulation with the opposing metal counter-bearing), rim (i.e. bearing periphery), non-articular (i.e. surfaces that are not intended for articulation with the opposing metal counter-bearing), and backside (i.e. the non-articular surfaces of modular bearings that are mated with metal baseplates).

The ability of inexperienced researchers to recognize and correctly identify the damage modes on the polyethylene bearings was evaluated after two training sessions. In the first session (Written Training), observers were provided written descriptions of the damage modes (Table 1), as would be available from a detailed literature search, and a brief (20 min) verbal explanation to clarify the modes' definitions and specific word meanings. In the second session (Atlas Training), observers were provided the Damage Mode Atlas (Tables 1, 2; Figs. 1, 2, 3) and a brief (20 min) verbal explanation of the characteristic visual features of each mode. Four observers trained in orthopaedic biomechanics, but without experience in the analysis of explanted polyethylene bearings, underwent Written Training and Atlas Training approximately 1 month apart. After each training session, each observer used the optical microscope to individually inspect a total of 161 marked regions on the selected bearings, identifying and recording the damage modes for each region. The experienced observer previously outlined these 161 regions using a fine-point (0.4 mm) marking pen and identified the associated damage modes, taking care not to include any of the regions used to create the Damage Mode Atlas. These marked regions were selected to represent the typical frequency distribution of damage modes reported for explanted polyethylene bearings with flat (infinite radius) to

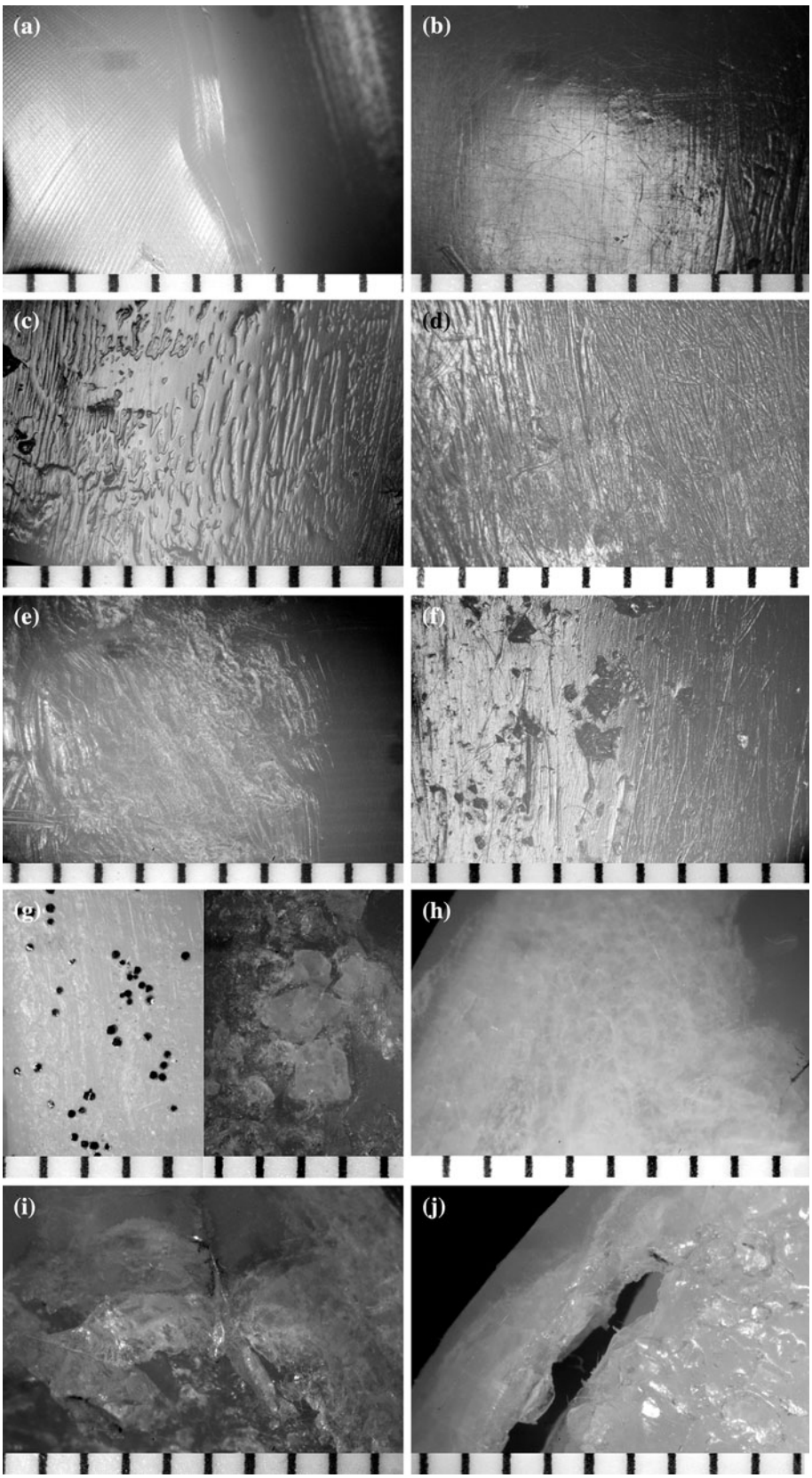

Fig. 1 Damage Mode Atlas images acquired through the microscope depicting damage modes consistent with adhesive/abrasive or fatigue mechanisms, including (**a**) non-articular deformation; (**b**) burnishing; (**c**) striations; (**d**) scratches: (**e**) abrasion; (**f**) pits; (**g**) embedded debris; (**h**) subsurface cracking; (**i**) delamination; (**j**) fracture. The scale below each image is calibrated in 1 mm intervals

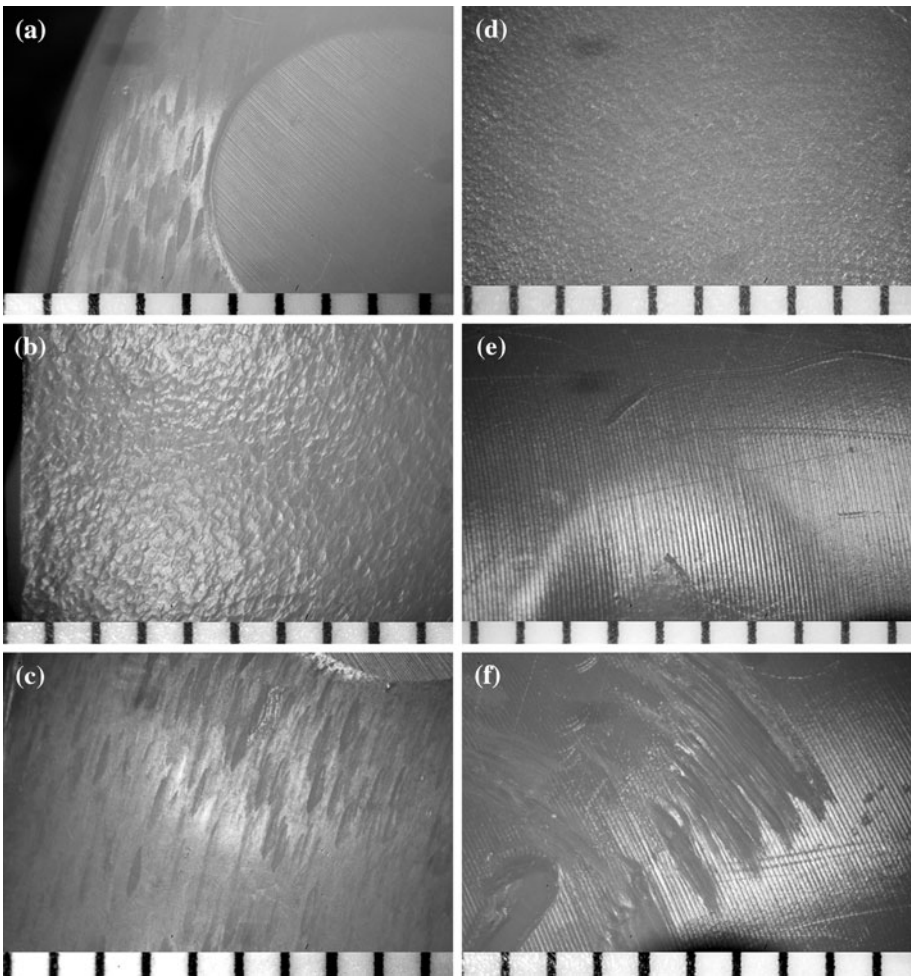

Fig. 2 Damage Mode Atlas images acquired through the microscope depicting modes characteristic of the non-articular (backside) surface of modular bearings ($n = 3$, left column), including (**a**) backside deformation within a field of stippling; (**b**) dimpling; (**c**) stippling; or common artifacts originating during surgery or manufacturing ($n = 3$, right column), including (**d**) processing artifacts; (**e**) visually indistinct; (**f**) tool damage. The scale below each image is calibrated in 1 mm intervals

moderately curved (40–80 mm radius) articular surfaces [4–6, 23]. Throughout the training sessions and subsequent inspections, the four observers were blind to the damage mode identification completed by the experienced observer. The selected bearings were evaluated in the same order for all observers, with the various damage modes randomly distributed among the marked regions.

The effectiveness of the Written Training and Atlas Training was assessed statistically. Metrics for each training session included the number of damage modes identified correctly by each observer and the length of time required to complete the evaluation of all marked regions. The marked regions were considered correctly identified if the damage mode recorded by the observer matched the damage mode previously recorded by the experienced observer. Changes in accuracy for each observer were evaluated by comparing the proportions of correctly identified regions in the two matched pair sessions (Written Training and Atlas Training) (McNemar's test). The inter-rater reliability, or agreement between the different observers, was evaluated using an intraclass correlation coefficient (Fleiss' κ).

3 Results

Implementing the Damage Mode Atlas into the training resulted in more accurate identification of the damage modes compared to written descriptions alone (Table 3). The number of regions with the damage mode correctly identified was consistent among the four observers (Fig. 4). Each observer had significantly greater proportions of correctly identified damage modes in the Atlas Training session compared to the Written Training session, increasing from $75 \pm 1\%$ (range, 75–76%) after the Written Training session to $92 \pm 2\%$ (range, 89–94%) after the Atlas Training session (McNemar's Test, $P < 0.001$). There was substantial improvement in the inter-rater reliability when the Damage Mode Atlas was used. All four observers correctly identified 79/161 (49%) regions after the Written Training session ($\kappa = 0.65$) and 134/161 (83%) regions after the Atlas Training session ($\kappa = 0.89$). There was correct identification by at least three observers in 114/161 (71%) regions and 146/161 (91%) regions after the Written Training and Atlas Training sessions, respectively. The average length of time required to complete the inspection was reduced by 45%,

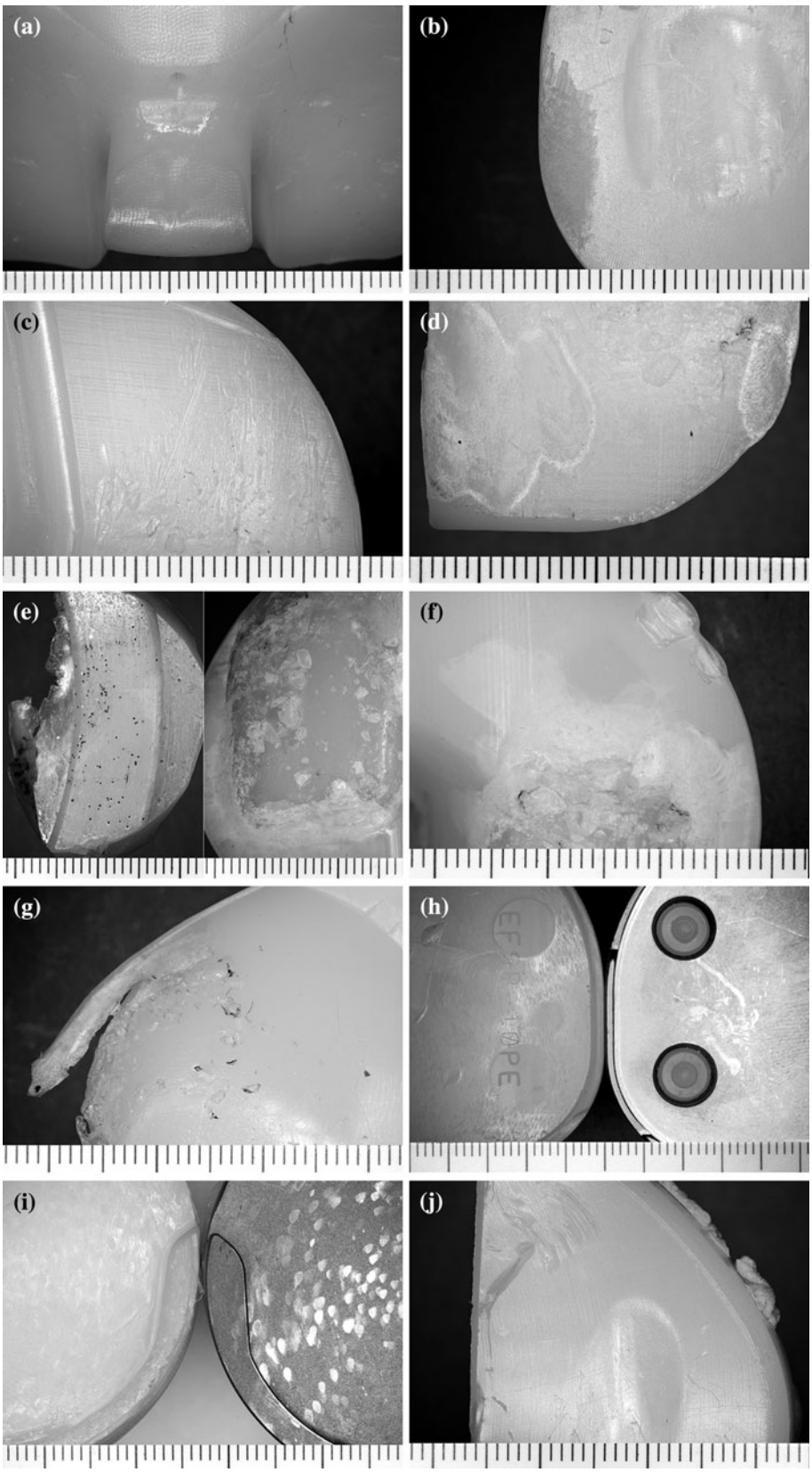

Fig. 3 Damage Mode Atlas images acquired as gross photographs depicting modes in which the relative size can be characterized as macro (i.e. visible to the unaided eye), including (**a**) non-articular deformation; (**b**) burnishing and abrasion; (**c**) scratches: (**d**) abrasion; (**e**) embedded debris; (**f**) subsurface cracking and surface delamination; (**g**) fracture; (**h**) backside deformation; (**i**) stippling; and (**j**) processing artifacts combined with tool damage and visually indistinct regions. The scale below each image is calibrated in 1 mm intervals

Table 1 Descriptions of distinct features characteristic for each damage mode, including the visual appearance under optical microscopy and typical mechanisms potentially contributing to the damage

Damage modes	Visual appearance	Typical mechanisms	References
Non-articular deformation	Visualized as a permanent change in shape not associated with condylar articulation	Compressive or shear load due to contact of the metal counter-bearing in non-articular regions	[4, 5, 7, 9, 12, 13, 23, 24, 33]
Burnishing	Visualized as smooth, highly polished regions that are highly reflective of incident light	Rolling contact of the metal counter-bearing	[4–6, 8, 11, 13, 14, 23, 24, 32, 33, 35, 36]
Striations	Visualized as highly oriented, longitudinal or dispersed, smooth peaks and troughs	High friction rolling and sliding contact of the metal counter-bearing	[4–6, 11, 23, 24]
Scratches	Visualized as thin lines in irregular or ordered directions	Sliding contact of the metal counter-bearing	[4–6, 13, 14, 23, 24, 32, 33, 35]
Abrasion	Visualized as rough, tufted regions with limited directionality	Sliding contact with bone or third-body cement debris or rough metal	[4–6, 13, 14, 23, 24, 32, 33, 35]
Pits	Visualized as depressions with rough surfaces and a typical diameter in the range of <1 mm up to 2 mm or greater	Material fatigue or fracture, or impressions from third body debris associated with component loosening	[4–6, 13, 23, 24, 32, 33, 36]
Embedded debris	Visualized as particles that differ in color and/or texture relative to the surrounding polyethylene surface, consistent with third-body particles of bone, cement fragments or metal	Third-body particles typically associated with component loosening or fracture	[5, 6, 13, 14, 23, 24, 33]
Subsurface cracking	Visualized as cracks and/or discoloration located inferior to the articular plane without surface discontinuity (rupture)	Fatigue, high sub-surface stress	[6, 15, 25]
Delamination	Visualized as thin layers of polyethylene material separated from the surface, with the remaining exposed material typically appearing textured and/or grossly pitted	Fatigue, high contact stress	[4–6, 8, 13, 15, 23–25, 32, 33]
Fracture	Visualized as complete cracks or wear-through of the polyethylene bearing, typically resulting in exposure of the metal baseplate or discontinuity of the bearing rim	Fatigue, high contact stress	[6, 8, 13, 23, 24]
Backside deformation	Visualized as permanent changes in shape typically observed around protrusions or screw holes existing on the metal baseplate	Compressive load deforming the polyethylene bearing against features on the metal baseplate	[5, 34, 36]
Dimpling	Visualized as uniform, nearly circular indentations approximately 100 μm in diameter that lack directionality	Compressive load deforming the polyethylene bearing against the textured metal baseplate	[5, 9]
Stippling	Visualized as unidirectional scratches approximately 1 mm or greater in length	Motion in the shear plane between the polyethylene bearing and metal baseplate	[35]
Processing artifacts (no damage)	Visualized as highly ordered and repeating patterns consisting of linear scratches (machine marks), uniform dimpled texture (molding), or a highly glossy surface (compression molding)	Contact with tools and molds during manufacturing	[9, 12]
Visually indistinct	Visualized as a disruption to machine marks or the original manufactured surface, but no clear damage mode can be distinguished microscopically	Infrequent contact with smooth articular surface of the metal counter-bearing	[23, 24]
Tool damage	Visualized as symmetric pattern with sharply distinct edges, or severe singular scratches or cuts that are incongruous with the surrounding damage modes	Grasping bearing with serrated surgical clamp, prying with chisel to disengage modular bearing, or contact with sharp saw or scalpel	[33]

Table 2 Five distinguishing features (descriptions in text) for each damage mode

Damage modes	Scale	Typical location	Color change	Texture	Reflectivity
Non-articular deformation	Macro	Non-articular	Absent	Smooth	High
Burnishing	Macro/micro	Articular	Absent	Smooth	High
Striations	Micro	Articular	Absent	Rough	High
Scratches	Macro/micro	Articular/rim/non-articular	Absent	Rough	Low
Abrasion	Macro	Articular/rim/non-articular	Present (opaque)	Rough	Low
Pits	Micro	Articular	Absent	Rough	Low
Embedded debris	Macro/micro	Articular/backside	Present	Rough	Low/high
Subsurface cracking	Macro	Articular/rim/non-articular	Present (opaque)	Smooth	Low/high
Delamination	Macro	Articular/rim/non-articular	Absent/present	Rough	Low
Fracture	Macro	Articular/rim/non-articular	Absent	Rough	Low
Backside deformation	Macro	Backside	Absent	None	Low
Dimpling	Micro	Backside	Absent	Rough	High
Stippling	Macro	Backside	Absent	Rough	Low
Processing artifacts (no damage)	Macro/micro	Articular/rim/non-articular	Absent	Rough/smooth[a]	Low/high
Visually indistinct	Macro	Articular	Absent	None	High
Tool damage	Macro	Rim/non-articular	Absent	Rough	Low

[a] Processing artifacts on the original surface serve as the reference control for texture

Table 3 The number of regions with the damage mode correctly identified after the Written Training and Atlas Training sessions

Damage modes	Count (% total)	Pre-training (% correct)	Post-training (% correct)
Processing artifacts (no damage)	6 (4%)	96	92
Visually indistinct	4 (2%)	31	31
Tool damage	6 (4%)	71	92
Burnishing	22 (14%)	89	100
Striations	22 (14%)	75	98
Scratches	25 (16%)	58	83
Abrasion	16 (10%)	63	91
Pits	21 (13%)	93	96
Embedded debris	4 (2%)	25	63
Subsurface delamination	6 (4%)	79	100
Delamination	9 (6%)	72	92
Fractures	5 (3%)	80	100
Non-articular deformation	5 (3%)	95	100
Backside deformation	3 (2%)	75	100
Dimpling	4 (2%)	94	94
Stippling	3 (2%)	83	100

Damage modes are grouped with those characteristic of common artifacts, those consistent with the adhesive/abrasive or fatigue mechanisms, and those characteristic of non-articular (backside) surface damage

from 157 ± 27 (129–188) minutes for Written Training to 87 ± 13 (range, 74–102) minutes for Atlas Training.

4 Discussion

Evaluation of medical devices retrieved after in vivo service provides unique evidence related to the physiological environment in which the biomaterials are expected to perform. In this study, a Damage Mode Atlas was developed as a reference guide of damage modes typically visualized on polyethylene bearings and was implemented as part of a training procedure for evaluating bearings after pre-clinical tests or after in vivo function. Utilizing the Damage Mode Atlas to train new researchers improved the damage pattern analysis, including more accurate

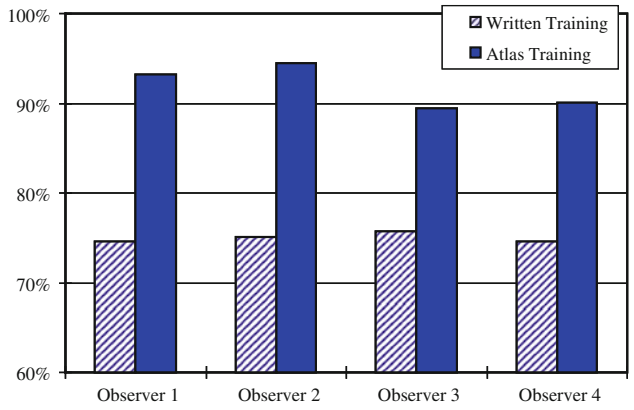

Fig. 4 Proportion of correctly identified damage modes for each observer after Written Training and Atlas Training

identification of damage modes and improved inter-rater reliability compared to written descriptions alone. International guidelines for standardized procurement and quantitative analysis of explanted devices are provided through ISO 12891 and ASTM F561, which generally describe three stages of progressively destructive analysis. This Damage Mode Atlas supplements stage II non-destructive analysis of explanted joint replacement bearings.

This study was motivated by a recognized absence of standardized reference materials for identifying specific damage modes and training researchers to complete damage pattern analysis of polyethylene bearings. Training researchers in such analysis necessarily requires the introduction of new vocabulary and unfamiliar technical concepts, and failure to use well-defined terminology can inhibit comprehension of detailed information and increase the risk of measurement errors. Moreover, not all researchers share a common language, which can further inhibit understanding of descriptions provided predominantly in English. Studies have shown that learning new words and concepts is strengthened when images are used with text to convey the meaning, helping to enhance memory and decrease task complexity [38]. Therefore, images were included in the Damage Mode Atlas to enhance comprehension during training and provide context to the visual appearance and typical damage mechanisms described for each damage mode (Table 1). The standardized terminology used to characterize five distinguishing features for each damage mode served to focus the observers on key distinctions between the modes (Table 2).

The Damage Mode Atlas was developed to guide objective assessments of prosthesis bearings manufactured from polyethylene. It was intended to provide reference images of damage modes that are readily visualized using common optical microscopy equipment widely available in a hospital-based setting. More complex imaging instrumentation (e.g. scanning electron microscope) was purposefully avoided since it is rarely available for routine screening of explants, does not allow efficient imaging of a large number of prostheses, and often requires specialized specimen preparation techniques which add to the cost burden for completing analysis. Similarly, a grading scale of damage severity was not included in the distinguishing features due to its recognized subjectivity [8] and the availability of more quantitative metrics (e.g. damage area, linear deformation) for assessing relative severity [4–6, 23, 39–41]. The Damage Mode Atlas is a considerably flexible tool, providing the possibility of adding more detailed images of the damage modes or additional damage categories specific to other biomaterials or prostheses with diverse geometry (e.g. acetabular cups or cervical disks). Moreover, it could be supplemented with clarification of additional damage mechanisms gained through other assessment techniques, as the typical damage mechanisms provided (Table 1) are not intended to represent the full spectrum of possible mechanisms that can generate damage in vivo.

The Damage Mode Atlas proved useful for training damage pattern analysis, but also demonstrated potential limitations for obtaining uniform data if adequate training is not achieved among different research groups studying polyethylene bearings. While the damage modes were correctly identified in 92% of the regions after the Atlas Training session, correct identification of all damage modes did not occur and accuracy was considerably lower for some specific damage modes (Table 3). Recognition of visually indistinct damage proved problematic and approximately one-third of the regions with this mode were incorrectly identified after Atlas training. However, the overall impact of this error is relatively low since visually indistinct damage occurs very infrequently on explanted prostheses and is more specific to bearings subjected to in vitro joint wear simulations [23, 24]. Difficulties recognizing embedded cement debris were also evident, typically resulting in the observers labeling the damage as pits or delamination, both of which were common to the embedded debris site on the specific bearings included. Considering reasons for revision that could generate third-body particles, such as loosening, or evidence of third-body wear on other explanted components submitted with a given polyethylene bearing (i.e. metal bearing with a scratched counter-face) can be helpful. Scratches were sometimes misidentified as abrasion or tool damage, which implies that the distinct mechanisms contributing to those latter two damage modes were not fully considered by the observers.

A limitation of this study involves the nature of training procedures. Improvements noted after Atlas Training (less time, better accuracy and reliability) could be due, in part,

to the experience each observer gained during the initial Written Training session. For this reason, training sessions were staged approximately 1 month apart in an effort to distinguish skills gained during Written Training from those gained during Atlas Training. The metric of evaluation time showed that most of the observers required progressively less time to complete the evaluations within a given session, and this affect was largely uniform for both training sessions. This suggests increased comfort in using the optical microscope and increased confidence in recognizing and identifying the different damage modes. In contrast, accuracy did not necessarily improve over the course of a given training session. During the Atlas Training session, accuracy in evaluating the final 81 regions was only 1–4% higher for three observers and was 2% lower for one observer compared to the initial 80 regions. Therefore, once an observer is trained to use the Damage Mode Atlas for studies involving explanted polyethylene bearings, accurate identification of damage modes can be achieved over the full study duration.

The terminology and images included in this Damage Mode Atlas are representative of common, existing descriptions of wear modes. The modes described (Table 1) were based on observations from 11 different research laboratories that were compiled from 19 different studies published in peer-reviewed scientific literature. These cited references are not meant to be exhaustive, nor representative of a formalized process for attaining consensus agreement among multiple research groups. Rather, widespread utilization of visual damage analysis suggests that this Damage Mode Atlas can serve as a practical template for recognizing damage features consistent with those elaborated in previous studies. In the absence of an international standard for naming and identifying the appearance of specific damage modes, this Damage Mode Atlas provides uniform descriptions and reference illustrations that are useful for consistent training of researchers.

It is recognized that the damage patterns characterized in this study are inclusive of mechanisms contributing to the liberation of material (i.e. wear), as well as mechanisms producing changes in the bearing surface without loss of material (i.e. creep deformation), consistent with previous studies [4, 13, 33]. The Damage Mode Atlas complements quantitative damage pattern analysis by aiding accurate identification of many localized regions of different damage modes on a given bearing surface [4–6, 11, 29]. As such, it is useful for verifying joint wear simulations and analytical models, and understanding the biomechanical function and debris-generating potential of prostheses under physiological conditions [4–6, 18, 23, 25–31]. Therefore, it is recommended that evaluation of polyethylene bearings from joint prostheses include training in damage pattern analysis facilitated by the use of the Damage Mode Atlas to complement both pre-clinical assessments and post-marketing surveillance.

Acknowledgments The authors acknowledge Kacper Juda, Wojciech Wojciechowski, and Ewa Bialoblocka for participating in training and data collection; Monica Montesi and Alina Beraudi for cleaning and archiving the explanted prostheses; Marzena Wojciechowicz for statistical advice; Michele Spinelli and Saverio Affatato for input during initial planning; and the surgeons from the Rizzoli Orthopaedic Institute who contributed explants to REPO. Financial support was received from a Marie Curie International Incoming Fellowship within the 7th European Community Framework Program (grant number PIIF-GA-2008-219978) and the Rizzoli Orthopaedic Institute.

References

1. Bozic KJ, Kurtz SM, Lau E, Ong K, Chiu V, Vail TP, Rubash HE, Berry DJ. The epidemiology of revision total knee arthroplasty in the United States. Clin Orthop Relat Res. 2010;468(1):45–51.
2. Kurtz SM, Muratoglu OK, Evans M, Edidin AA. Advances in the processing, sterilization, and cross-linking of ultra-high molecular weight polyethylene for total joint arthroplasty. Biomaterials. 1999;20:1659–88.
3. Wright TM. Polyethylene in knee arthroplasty: what is the future? Clin Orthop Relat Res. 2005;440:141–8.
4. Harman MK, Banks SA, Hodge WA. Polyethylene damage and knee kinematics after total knee arthroplasty. Clin Orthop Relat Res. 2001;392:383–93.
5. Harman MK, Banks SA, Hodge WA. Backside damage corresponding to articular damage in retrieved polyethylene tibial inserts. Clin Orthop Relat Res. 2007;458:137–44.
6. Harman MK, Schmitt S, Banks SA, Viceconti M, Hodge WA. Polyethylene damage and deformation on fixed-bearing, nonconforming unicondylar knee replacements corresponding to progressive changes in alignment and fixation. Clin Biomech. 2010;25(6):570–5.
7. Banks SA, Harman MK, Hodge WA. Mechanism of anterior impingement damage in total knee arthroplasty. J Bone Joint Surg Am. 2002;84(suppl 2):37–42.
8. Blunn GW, Joshi AB, Minns RJ, Lidgren L, Lilley P, Ryd L, Engelbrecht E, Walker PS. Wear in retrieved condylar knee arthroplasties: a comparison of wear in different designs of 280 retrieved condylar knee prostheses. J Arthroplast. 1997;12:281–90.
9. Silva M, Kabbash CA, Tiberi JV, Park SH, Reilly DT, Mahoney OM, Schmalzried TP. Surface damage on open box posterior stabilized polyethylene tibial inserts. Clin Orthop Relat Res. 2003;416:135–44.
10. Wasielewski RC, Galante JO, Leighty RM, Natarajan RN, Rosenberg AG. Wear patterns on retrieved polyethylene tibial inserts and their relationship to technical considerations during total knee arthroplasty. Clin Orthop Relat Res. 1994;299:31–43.
11. Wimmer M, Andriacchi T, Natarajan R, Loos J, Karlhuber M. A striated pattern of wear in ultrahigh-molecular-weight polyethylene components of Miller-Galante total knee arthroplasty. J Arthroplast. 1998;13(1):8–16.
12. Willie BM, Foot LJ, Prall MW, Bloebaum RD. Surface damage analysis of retrieved highly crosslinked polyethylene tibial components after short-term implantation. J Biomed Mater Res (Appl Biomater). 2008;85(1):114–24.
13. Gunther SB, Graham J, Norris TR, Ries M, Pruitt L. Retrieved glenoid components: a classification system for surface damage analysis. J Arthroplast. 2002;17(1):95–100.

14. Hertel R, Ballmer FT. Observations on retrieved glenoid components. J Arthroplast. 2003;18(3):361–6.
15. Bloebaum RD, Nelson K, Dorr L, Hofmann AA, Lyman DJ. Investigation of early surface delamination observed in retrieved heat-pressed tibial inserts. Clin Orthop Relat Res. 1991;269: 120–7.
16. Collier MB, Engh CA, McAuley JP, Engh GA. Factors associated with the loss of thickness of polyethylene tibial bearings after knee arthroplasty. J Bone Joint Surg Am. 2007;89(6):1306–14.
17. Fehring TK, Murphy JA, Hayes TD, Roberts DW, Pomeroy DL, Griffin WL. Factors influencing wear and osteolysis in press-fit condylar modular total knee replacements. Clin Orthop Relat Res. 2004;428:40–50.
18. Hirakawa K, Bauer TW, Yamaguchi M, Stulberg BN, Wilde AH. Relationship between wear debris particles and polyethylene surface damage in primary total knee arthroplasty. J Arthroplast. 1999;14(2):165–71.
19. McGovern TF, Ammeen DJ, Collier JP, Currier BH, Engh GA. Rapid polyethylene failure of unicondylar tibial components sterilized with gamma irradiation in air and implanted after a long shelf life. J Bone Joint Surg Am. 2002;84(6):901–6.
20. Nyffeler RW, Werner CML, Simmen BR, Gerber C. Analysis of a retrieved Delta III total shoulder prosthesis. J Bone Joint Surg Br. 2004;86(8):1187–91.
21. Rockwood CA, Wirth MA. Observation on retrieved Hylamer glenoids in shoulder arthroplasty: problems associated with sterilization by gamma irradiation in air. J Shoulder Elbow Surg. 2002;11(2):191–7.
22. Scarlat MM, Matsen FA. Observations on retrieved polyethylene glenoid components. J Arthroplast. 2001;16(6):795–801.
23. Harman MK, DesJardins J, Benson L, Banks SA, LaBerge M, Hodge WA. Comparison of polyethylene tibial insert damage from in vivo function and in vitro wear simulation. J Orthop Res. 2009;27(4):540–8.
24. Harman MK, Affatato S, Spinelli M, Zavalloni M, Stea S, Toni A. Polyethylene insert damage in unicondylar knee replacement: comparison of in vivo function and in vitro simulation. Proc Inst Mech Eng. 2010;224(7):823–30.
25. Blunn GW, Walker PS, Joshi A, Hardinge K. The dominance of cyclic sliding in producing wear in total knee replacement. Clin Orthop Relat Res. 1991;273:253–60.
26. Cornwall GB, Bryant JT, Hansson CM. The effect of kinematic conditions on the wear of ultrahigh molecular weight polyethylene (UHMWPE) in orthopaedic bearing applications. Proc Inst Mech Eng H. 2001;215(1):95–106.
27. Fregly BJ, Sawyer WG, Harman MK, Banks SA. Computational wear prediction of a total knee replacement from in vivo kinematics. J Biomechanics. 2005;38:305–14.
28. Rawlinson JJ, Furman BD, Li S, Wright TM, Bartel DL. Retrieval, experimental, and computational assessment of the performance of total knee replacements. J Orthop Res. 2006; 24(7):1384–94.
29. Tamura J, Clarke IC, Kawanabe K, Akagi M, Good VD, Williams PA, Masaoka T, Schroeder D, Oonishi H. Micro-wear patterns on UHMWPE tibial inserts in total knee joint simulation. J Biomed Mater Res. 2002;61(2):218–25.
30. Hopkins AR, Hansen UN, Amis AA, Knight L, Taylor M, Levy O, Copeland SA. Wear in the prosthetic shoulder: association with design parameters. J Biomech Eng. 2007;129(2):223–30.
31. Swieszkowski W, Bednarz P, Prendergast PJ. Contact stresses in the glenoid component in total shoulder arthroplasty. Proc Inst Mech Eng H. 2003;217(1):49–57.
32. Hood RW, Wright TM, Burstein AH. Retrieval analysis of total knee prostheses: a method and its application to 48 total condylar prostheses. J Biomed Mater Res. 1983;17:829–42.
33. Wright TM, Rimnac CM, Faris PM, Bansal M. Analysis of surface damage in retrieved carbon fiber-reinforced and plain polyethylene tibial components from posterior stabilized total knee replacements. J Bone Joint Surg Am. 1988;70:1312–9.
34. Conditt MA, Thompson MT, Usrey MM, Ismaily SK, Noble PC. Backside wear of polyethylene tibial inserts: mechanism and magnitude of material loss. J Bone Joint Surg Am. 2005;87(2): 326–31.
35. Rao A, Engh G, Collier M, Smain L. Tibial interface wear in retrieved total knee components and correlations with modular insert motion. J Bone Joint Surg Am. 2002;84(10):1849–55.
36. Surace MF, Berzins A, Urban RM, Jacobs JJ, Berger RA, Natarajan RN, Andriacchi TP, Galante JO. Back surface wear and deformation in polyethylene tibial inserts retrieved postmortem. Clin Orthop Relat Res. 2002;404:14–23.
37. Hyzer WG, Krauss TC. The bite mark standard reference scale: ABFO No. 2. J Forensic Sci. 1988;33(2):498–506.
38. Vesely P, Gryder N. Teaching visual imagery for vocabulary learning. Acad Exch Q. 2007;11(2):51–5.
39. Grochowsky JC, Alaways LW, Siskey R, Most E, Kurtz SM. Digital photogrammetry for quantitative analysis of retrieved TKA components. J Biomed Mater Res B Appl Biomater. 2006; 79(2):263–7.
40. Spinelli M, Carmignato S, Affatato S, Viceconti M. CMM-based procedure for polyethylene non-congruous unicompartmental knee prosthesis wear assessment. Wear. 2009;267:753–6.
41. Blunt LA, Bills PJ, Jiang XQ, Chakrabarty G. Improvement in the assessment of wear of total knee replacements using coordinate-measuring machine techniques. Proc Inst Mech Eng H. 2008;222(3): 309–18.